



Vasculogenic mimicry-associated novel gene signature predicted prognosis and response to immunotherapy in lung adenocarcinoma

Lei Zhang^{a,1}, Jiatao Wu^{b,1}, Wei Wei Yin^{c,1}, Junjie Hu^d, Lingli Liao^e, Junjie Ma^f, Ziwei Xu^f, Shiwu Wu^{b,g,*}

^a Department of General Surgery, the Second Affiliated Hospital of Bengbu Medical University, Anhui Province 233080, China

^b Anhui Province Key Laboratory of Clinical and Preclinical Research in Respiratory Disease, Molecular Diagnosis Center, First Affiliated Hospital, Bengbu Medical University, 287 Changhuai Road, Anhui, Bengbu 233004, China

^c Department of Thoracic Surgery, the Second Affiliated Hospital of Bengbu Medical University, Anhui Province 233080, China

^d Department of Radiotherapy, the Second Affiliated Hospital of Bengbu Medical University, Anhui Province 233080, China

^e Department of Clinical Nutrition, the First People's Hospital of Yibin, Sichuan Province 644000, China

^f Bengbu Medical University, Anhui Province 233030, China

^g Anhui No. 2 Provincial People's Hospital, Hefei 230041, China

ARTICLE INFO

Keywords:

Vasculogenic Mimicry
Lung Adenocarcinoma
Prognosis
Immunotherapy
ANLN

ABSTRACT

Backgrounds: It was highlighted by recent studies on the biological significance of vasculogenic mimicry (VM) in tumorigenicity and progression. However, it is unclear whether VM also plays a potential role in immune regulation and tumor microenvironment (TME) formation.

Methods: To identify patterns of VM alterations and VM-associated genetic features in non-small cell lung adenocarcinoma, we have screened 309 VM regulators and performed consensus molecular typing by the NMF algorithm. The ssGSEA and CIBORSORT algorithms were employed to measure the relative infiltration of distinct immune cell subpopulations. Individual tumors with immune responses were evaluated for alteration patterns of VM with typing-based differential genes.

Results: In 490 LUAD samples, two distinctive VM alteration patterns connected to different clinical outcomes and biochemical pathways were established. TME characterization showed that the observed VM patterns were primarily saturated with cell proliferation and metabolic pathways and higher in immune cell infiltration of the C1 type. Vasculogenic mimicry-related genes (VMRG) risk scores were constructed to divide patients with lung adenocarcinoma into subgroups with high and low scores. Patients with lower scores had better immunological scores and longer survival times. Upon further investigation, higher scores were positively correlated with higher tumor mutation burden (TMB), M1-type macrophages and immune checkpoint molecules. Nevertheless, in two other immunotherapy cohorts, individuals with lower scores had enhanced immune responses and long-lasting therapeutic benefits. Finally, we monitored the ANLN gene from the VMRG model, which was highly expressed in lung adenocarcinoma tissues and negatively correlated with prognosis; it was also highly expressed in lung adenocarcinoma cell lines, and knockdown of ANLN elicited low expression of VEGFA, MMP2 and MMP9.

Conclusion: This study highlights that VM modifications are significantly associated with the diversity and complexity of TME, revealing new features of the immune microenvironment in lung adenocarcinoma and providing a new strategy for immunotherapy. Screening ANLN as a critical target for vasculogenic mimicry in lung adenocarcinoma provides a novel perspective for the targeted treatment of lung adenocarcinoma.

1. Introduction

Lung adenocarcinoma (LUAD) is the primary cause of cancer-related

deaths worldwide, and adenocarcinoma is its leading pathological type, accounting for more than 40% of cases [1]. Although treatment options are diverse and advances have been implemented, the 5-year overall

* Corresponding author.

E-mail address: 13705523357@163.com (S. Wu).

¹ Author contributed equally

<https://doi.org/10.1016/j.prp.2023.155048>

Received 12 May 2023; Received in revised form 18 August 2023; Accepted 24 August 2023

Available online 21 December 2023

0344-0338/© 2023 Elsevier GmbH. All rights reserved.

survival (OS) rate for LUAD still remains below 20%[2]. At present, the prognosis-related mechanisms of LUAD have not yet been elucidated. Tumor invasion and metastasis are closely related to tumor angiogenesis, which has become one of the most widespread problems in oncology[3]. Therefore, it remains a significant challenge to accurately individualize the assessment and improve the survival of LUAD patients.

Solid tumor formation depends on a continuous supply of oxygen and nutrients[4]. Angiogenesis has a crucial role in tumor development because of its constant supply of oxygen and nutrients to the tumor, and tumor cells may also use this circulatory pathway to allow patients to develop recurrence and metastasis[5,6]. Throughout the years, a lot of attention has been focused on the function of budding angiogenesis or reaggregation of vascular endothelial cells from the surrounding pre-existing vessels to the tumor[7]. However, in addition to endothelium-dependent angiogenesis, Maniotis first identified a novel model of tumor blood supply in human melanoma, called vasculogenic mimicry (VM), which is a novel endothelium-independent mode of tumor blood supply consisting of a tubular network of pluripotent and stem cell-like (both tumor and endothelium) phenotypes of cancer cells that provide sufficient solid tumor growth blood supply[8]. It has been found that VM tubular walls stained positive for periodic acid-Schiff (PAS) and negative for endothelial cell markers such as CD31 and CD34, indicating that VM tubular walls are not composed of endothelial cells but directly of tumor cells[8,9]. This tubular pattern provided sufficient blood supply for malignant tumors and is essential to tumor growth and metastasis. This ductal pattern provides adequate blood supply to malignant tumors and plays a critical role in their development and metastasis.

Recent studies have revealed the interaction between VM and the tumor immune microenvironment, which provides a new perspective on the interaction between VM and tumor immune cells[10]. Liu et al. reported that melanoma cells with high NGFR expression possess a vasculogenic mimicry phenotype and highly express PD-L1 close to immune cells[11]. Wang et al. also reported that MAGEA3 promotes the formation of tumor vasculogenic mimetic[12]. The immune microenvironment was then remodeled. Tumor stem cells, cancer-associated fibroblasts, and tumor-associated macrophages in the immune microenvironment can promote VM spontaneously or secondarily[13–15]; yet, there is still a lack of effective targets to inhibit VM formation. In this study, we constructed a spanning three-classification molecular typing of LUAD utilizing genes correlated with VM generation from the GEO database, consisting of ANLN, ABCA3 and SFTA3 together. Further analysis revealed that ANLN was significantly upregulated in LUAD and its high expression was negatively correlated with prognosis. By constructing ANLN knockdown lung adenocarcinoma cell lines, we examined the expression levels of VM-related proteins VEGFA, MMP2 and MMP9 and found that all appeared to be down-regulated. It can be concluded that ANLN can be a crucial target for the formation of LUAD angiogenic mimics, and inhibition of ANLN can effectively prevent the progression of LUAD.

2. Materials and Methods

2.1. Collect and Preprocess Publicly Available Expression Datasets

Gene expression data and clinical characteristics of LUAD samples were retrospectively collected from publicly available datasets from the NCBI GEO database (<https://www.ncbi.nlm.nih.gov/geo/>) and TCGA (<https://cancergenome.nih.gov/>). Total 594 TCGA-LUAD (The Cancer Genome Atlas-Non-Small Cell Lung Adenocarcinoma Cancer, N = 594) patients were incorporated into the analysis, in addition to the GSE43742 cohort (N = 4), GSE37892 (N = 12), and GSE179975 (N = 6) datasets. Since these GEO datasets share the same microarray sequencing platform (AffymetrixHG-U133 +2.0), we downloaded the original "CEL" files and processed them with the "affy" and The background noise adjustment and batch effect correction were performed by

the "Simple Processing" package. Batch effects between different GEO datasets were removed using the ComBat method in the "SVA" R package. Genomic mutation data for TCGA-LUAD were obtained from the UCSC Xena database and Davoli et al. Non-synonymous mutations (including shift mutations, missense mutations, nonsense mutations and splice site mutations) counts identified as TMB.

2.2. Consensus molecular clustering of VM regulators by NMF. An NMF consensus clustering was performed using three GEO microarray intersection genes

Specifically, the expression of 309 VM regulators (MatrixA) was decomposed into two non-negative matrices W and H (i.e., $A \approx WH$). The decomposition of MatrixA was repeated and its output was aggregated to obtain the consensus clustering of lung adenocarcinoma samples. The optimal number of clusters is selected based on the coeval coefficient, dispersion coefficient and contour coefficient. Consensus clustering was performed using the R package "NMF" (version 0.22.0) with the brunet algorithm and 200 runs.

2.3. Estimation of Tumor-Microenvironment Cell Infiltration

The cell sorting algorithm (<https://cibersort.stanford.edu/>) was used to estimate the relative abundance of 22 different immune cell types based on gene expression in tumor tissues[16]. We also applied the microenvironmental cell population counter (MCPCounter) method using the R package "MCPCounter" to quantify the absolute abundance of eight immune cell populations and two stromal cell populations in tumor tissues from RNA-seq data. Univariate Cox regression analysis was further performed on cell types that differed significantly between tumors with high and low VMRG to determine their correlation with overall survival using the best group cut-off values.

2.4. Gene set variation analysis (GSVA) and gene ontology (GO) annotation

A GSVA analysis and the R package "GSVA" were used to study the variation of biological processes between different VM modification patterns[17]. Explicit biological signatures were obtained from the signature marker gene set (downloaded from MSigDB database v7.1) and the gene set constructed by Maritassan et al. (from the IMvigor210 synergistic biopackage).

2.5. Adopting ssGSEA Immune Cell Infiltration Estimation and Inverse Fold Product Algorithm

Single sample gene set enrichment analysis (ssGSEA) to quantify the relative abundance of 28 immune cell types in the tumor microenvironment. The specific panel of signature genes used to mark each immune cell type was compiled from a recent study. The relative abundance of each immune cell type was expressed as an enrichment score in the ssGSEA analysis and normalized to a uniform distribution from 0 to 1. The Biosimilarity of infiltrating immune cells was estimated using multidimensional scaling (MDS) and Gaussian fitting models. The abundance of 22 different leukocyte subpopulations was estimated using the inverse fold product method of Western cell classification (<http://cibersort.stanford.edu/>).

2.6. Quantitative Immune Response Predictors, Immunoscope (Immunophenoscore), TIDE and ESTIMATE

Immunophenoscore (IPS) is a superior predictor of response to anti-CTLA-4 and anti-PD-1 regimens. It quantifies the determinants of tumor immunogenicity and characterizes the intratumoral immune landscape and cancer antigenome, belonging to a scoring scheme developed by a panel of immune-related genes. MHC-related molecules (MHC),

checkpoints or immunomodulators (CP), effector cells (EC) and suppressor cells (SC). Weighted average Z-score, The weighted average Z-score, was calculated by averaging the sample Z-scores of the four categories in their respective categories. The weighted average Z-score was calculated by averaging the Z-scores of the four categories in their separate categories and the sum of the weighted average Z-scores was calculated as IPS. The tumor immune dysfunction and rejection (TIDE) algorithm proposed by Jiang et al. was used to model different tumor immune evasion mechanisms, including Dysfunction of tumor-infiltrating cytotoxic T lymphocytes (CTLs) and rejection of CTLs by immunosuppressive factors, rejection by immunosuppressive factors [18]. A higher TIDE score indicates that tumor cells are more likely to induce immune escape, thus indicating a lower response rate to ICI. Estimating stromal and immune cells in malignant tumors uses the Expression Data Estimation of Stromal and Immune Cells in Malignant Tumors (ESTIMATE) algorithm, which uses the unique properties of transcriptional profiles to infer the cellularity of tumors and the purity of tumors. By using the ESTIMATE algorithm, we calculated immune and stromal scores to predict the levels of infiltrating immune and stromal, which form the basis of tumor purity. Tumor tissue with a large number of immune cell infiltrates represents a higher immune score and lower tumor purity.

2.7. Mutation Characteristics of Significantly Mutated Genes and Tumors

The mutational landscape of VM-modified genes and smg in the TCGA-LUAD cohort was described by the waterfall function of the R 'maftools' package. Mutation signatures extracted from TCGA genomic data were also used in the 'maftools' package. The extracted signature function based on Bayesian variable non-negative matrix decomposition decomposes the mutation portrait matrix into two non-negative matrices "signature" and "contribution", where "signature" represents the mutation. The "signature" represents the mutation process and the "contribution" represents the corresponding mutation activity. The signature enrichment function automatically determines the optimal number of extracted mutation signatures and assigns them to each sample based on mutation activity. The extracted CC mutation profiles were compared and annotated with the cancer somatic mutation catalog (universe) by cosine similarity analysis.

2.8. Construction of a prognostic model for vasculogenic mimicry-related genes

A previous consensus clustering algorithm classified patients into two different VM modification patterns, and we next identified VM modification-related differentially expressed genes (DEGs) in different VM phenotypes. The R package 'limma' was used to evaluate deg in LUAD samples between different modification clusters. Specifically, gene expression data were normalized by voom and entered into the limit and eBayes functions to calculate the differential expression statistics. The significance filtering criteria for deg was set to an adjusted p-value of less than 0.001. the TCGA set was divided using the 'caret' R package. Ultimately, 236 and 232 patients were included in the training set (construction of the model) and the test set (validation of the model), respectively. We constructed three VM-related gene scores (VMRG) by least absolute shrinkage and selection operator (LASSO) Cox regression analysis using the "glmnet" package of R. The relationship between VM-associated genes and LUAD risk was used to assess the association according to the following equation: Risk score = $\sum(\beta_i^* \text{Exp}_i)$. Clinical information and platform annotation information for the external validation dataset were obtained from the GSE30219 dataset of the Gene Expression Omnibus (GEO) database (<http://www.ncbi.nlm.nih.gov/geo>). A total of 307 LUAD patients were included in the validation dataset of this study.

2.9. Single-cell RNA sequencing

The processed single-cell data were integrated by the "Seurat" package to identify anchor points, and firstly, cells and genes included in this study were filtered according to the following criteria: 1) cells expressing less than 200 genes were removed; 2) genes expressed in less than three cells were removed. 3) cells expressing genes fluctuating between 200 and 7000 genes were retained. 7000 genes were retained. 4) Cells with less than 10% of mitochondrial genes were retained. The Sc transform function was used to eliminate the effect of the cell cycle on subsequent results. The number of selected dimensions was set to 20. The first 20 principal components were selected for cluster analysis by K-nearest neighbor (KNN). Cells were divided into three subgroups immune, epithelial and stromal cells by manually selecting the marker genes of the cells. Since ANLN is highly expressed in epithelial cells, we speak about epithelial cells were sorted out for re-clustering.

2.10. Cell Lines and Culture

Human normal bronchial epithelial cells (BEAS-2B) and three human lung adenocarcinoma cell lines (A549, H1975 and PC9) were purchased from the Chinese Academy of Sciences cell bank, Shanghai Branch. All cell lines were grown in RPMI-1640 medium supplemented with 10% fetal bovine serum (FBS) and 1% (v/v) penicillin and streptomycin and cultured at 37 °C in a humidified environment with 5% CO₂.

2.11. siRNA transfection

Three pairs of ANLN gene siRNA fragments (siANLN-1, siANLN-2 and siANLN-3) and one pair of non-targeting control siRNA fragments (si-NC) were designed and synthesized. To down-regulate ANLN expression, small interfering RNAs (si-NC, siANLN-1, siANLN-2 and siANLN-3) were introduced into non-small cell lung cancer cells. When the cell fusion rate reached 50%–60%, Lipofectamine® 3000 reagent (Thermo Fisher Science) was used according to the operation manual. Cell transfection was performed to suppress the expression of endogenous ANLN. RT-PCR and Western blotting were performed to detect the knockdown efficiency of siRNAs.

2.12. Western blot and qRT-PCR

Proteins were extracted from the cells using RIPA strong lysis buffer. Equal amounts of protein samples were separated by SDS-PAGE and transferred to PVDF membranes. PVDF membranes were closed in TBST-prepared 5% skim milk at room temperature for one hour. Then, the membranes were incubated with diluted primary antibodies on a shaker overnight at 4 °C (All antibodies were obtained from Proteintech). Then, the membranes were washed three times with TBST, followed by incubation with the corresponding secondary antibodies at room temperature for one hour, rinsed again with TBST, and finally developed with Gel Doc 2000 (Bio-Rad). Total RNA from A549 and PC9 cells was extracted using TRIzol kit (Thermo Fisher Science) and complementary DNA (cDNA) was synthesized using PrimeScrip RT kit (Takara, Japan). The qRT-PCR experiments were performed using a Roche 480 machine to obtain the Ct values of the amplified products, and the final results were normalized to the expression of actin (β -actin). Gene expression was quantified using the 2- $\Delta\Delta$ CT method.

2.13. Statistical Analysis

All statistical analyses were performed using R software (version 4.1.3, <http://www.r-project.org>). Kaplan-Meier curves and log-rank tests were used to compare the survival outcomes of the subgroups. The independent prognostic value of OS clinical characteristics was assessed using a univariate Cox proportional risk regression analysis. The prognostic power of the OS prediction model was evaluated using

subject operating characteristic (ROC) curves (R package "timeROC") and area under the curve (AUC) values. Differences between groups were compared using an independent samples t-test. P value < of 0.05 was considered statistically significant[19].

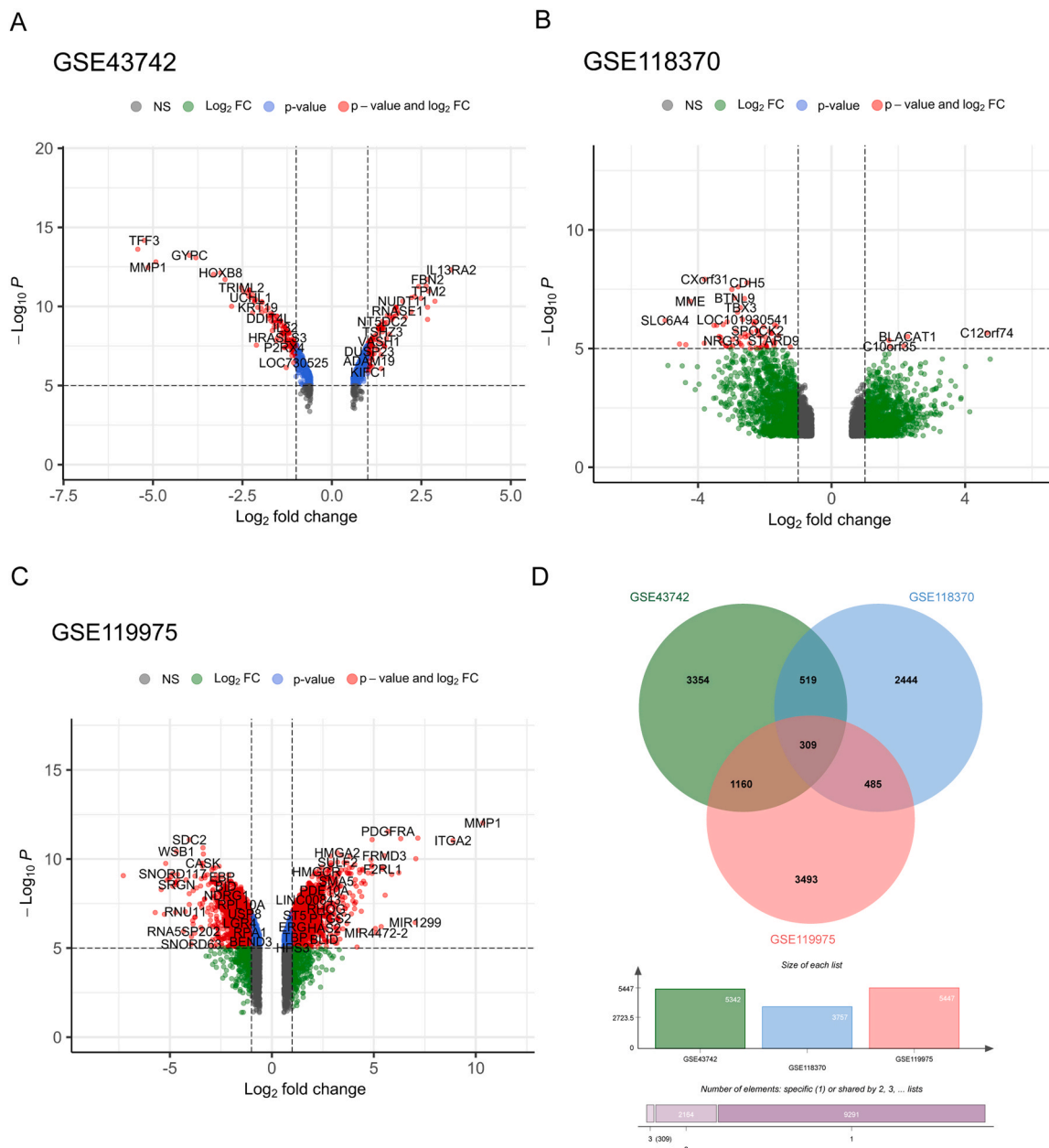
3. Results

3.1. Filtration and identification of vasculogenic mimicry-related genes

Angiogenesis-related microarrays were acquired from the GEO dataset with three microarrays GSE43742, GSE118370, GSE119975 respectively for differential genes ($|\log_2FC| > 0.585, p < 0.05$). 5342, 3757 and 5447 differential genes were obtained, respectively (Fig. 1A-C), and Venn diagrams were plotted to obtain intersection sets for obtaining 309 vasculogenic mimicry-related genes in lung cancer (Fig. 1D).

3.2. Consensus clustering to identify different subgroups and inter-cluster prognostic analysis

The 309 vasculogenic mimicry-related genes obtained by GEO were first analyzed for differences in LUAD ($|\log_2FC| > 1, p < 0.05$), and a total of 51 genes with significant LUAD differences were obtained (Table S1). Then, microarray data of LUAD gene expression were merged with clinical data, and finally 490 LUAD samples with survival times were identified for consistent clustering. Specifically, the 51 VM-related expressions were decomposed into two non-negative matrices. Repeated decomposition of the matrices and aggregation of their outputs were performed to obtain consistent clustering of LUAD samples (Supplementary Figure 1). The optimal number of clusters was selected based on the coeval, dispersion, and contour coefficients. Consensus clustering was performed using the R package "NMF" (version 22.0) with the Blue Meta algorithm and 200 runs (Fig. 2A-B). The results of Kaplan-Meier survival analysis showed a significant difference between C1 and C2



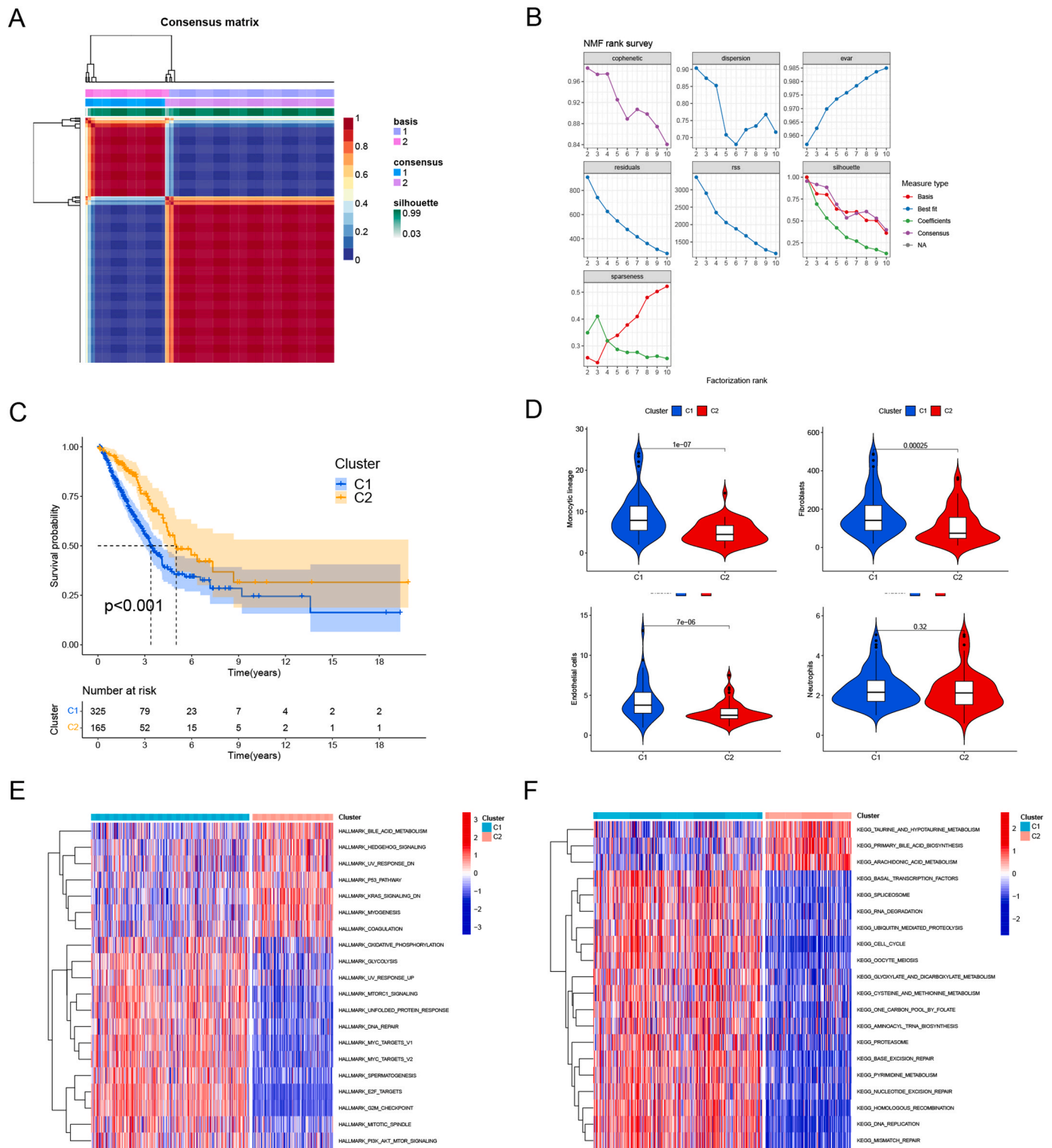


Fig. 2. VM modification pattern and relevant biological pathway. (A) Nonnegative matrix factorization (NMF) clustering was conducted and two subgroups were identified the optimal value for consensus clustering. (B) Factorization rank for $k = 2-10$. (C) Kaplan-Meier curves of overall survival (OS) for 490 LUAD patients in the TCGA cohort with two VM clusters. The numbers of patients in VM-C1 and VM-C3 phenotypes are 325 and 165, respectively (Log-rank test). The VM-C1 showed significantly worse prognostic than VM-C1 cluster in TCGA-LUAD cohorts. (D) Differences between the two types of immune cells in the MCPcounter algorithm. (E-F) Heatmap shows the GSEA score of representative Hallmark and KEGG pathways curated from MSigDB in distinct VM modification patterns.

($p < 0.05$). The samples in cluster 2 outperformed the samples in cluster 1 in terms of OS ($p < 0.05$, Fig. 2C). To further elucidate the differences between the two molecular subtypes of LUAD in immune cells, we calculated the degree of infiltration of 10 immune cells in TCGA_LUAD

patients by the MCPcounter algorithm and compared the differences between the two immune cells in the two clusters. The results showed that some immunosuppressive cells in bone marrow dendritic cells, endothelial cells, fibroblasts and monocytes infiltrated in higher

abundance in C1 than in C2, CD8 + T cells and neutrophils did not differ in the two subgroups ($p < 0.05$, Fig. 2D). Immune-activated cytotoxic lymphocytes, CD8 + T cells, T lymphocytes and NK cells were infiltrated in higher abundance in C1 than in C2 ($p < 0.05$, Supplementary Figure 2A-F). To clarify the difference in pathway expression between C1 and C2, we performed GSVA analysis using two datasets, HALLMARK and KEGG, respectively, which showed that C1 with poor prognosis was enriched in oxidative phosphorylation pathway, mismatch repair pathway and some pathways that promote cell proliferation, and C2 with good prognosis was enriched in p53 pathway and HEDGEHOG pathway (Fig. 2E-F). The above results suggest that molecular typing based on vasculogenic mimicry for LUAD reconstitution is useful for predicting LUAD prognosis and assessing tumor immune microenvironment.

3.3. Construction and identification of LUAD prognostic models based on angiogenic mimetic molecular typing

Primary steps were performed to identify the differences in gene expression profiles between the two typologies C1 and C2 ($|\log_{2}FC| > 1$, $p < 0.05$), and a total of 141 differential genes were obtained (Table S2). A total of 126 LUAD prognosis-related genes were obtained using univariate Cox regression analysis (Table S3). The characteristics of LUAD prognosis prediction were established using LASSO Cox regression, and VM-associated gene risk scores were determined using the three most relevant genes (Supplementary Figure 3A-B) - VMRG. risk scores were calculated as follows: risk score = (0.417 * ANLN expression) + (-0.114 * ABCA3 expression) + (-0.1 * SFTA3 expression). The TCGA_LUAD samples were randomly grouped 7:3, where seven was set as the training set, three was set as the test set, and GSE30219 (N = 307) was selected as the external validation set. The samples were risk scored

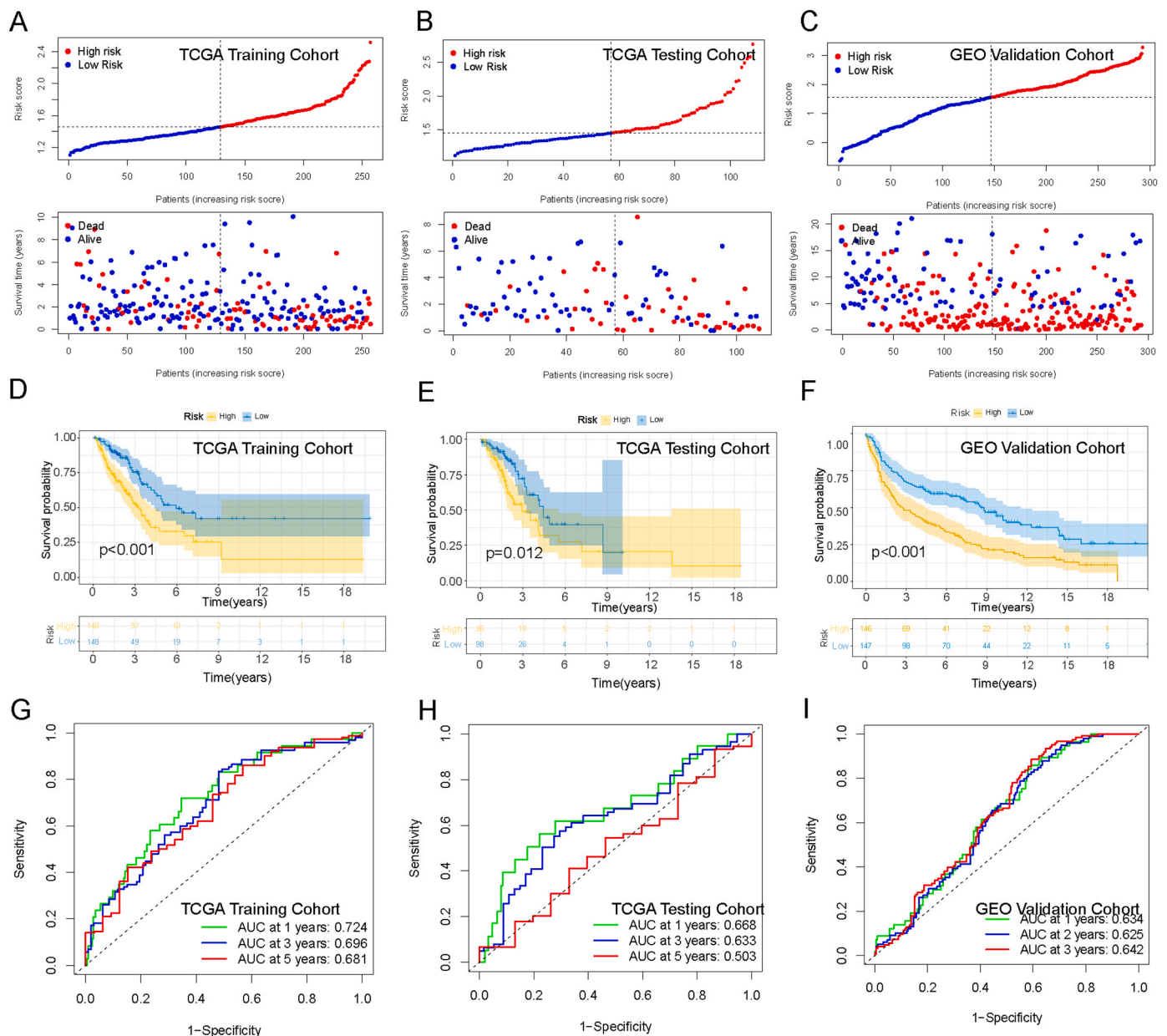


Fig. 3. Construction and verification of the VM-related risk model by Lasso-Cox regression analysis. (A-C) Distribution of risk curves and number of patients in VMRG risk score. (A) Train Set; (B) Test Set; (C) External Validation Set. (D-F) Kaplan-Meier curves for patients with high and low VMRG subgroups. (D) Train Cohort; (E) Test Cohort; (F) GEO cohort; (G-I) ROC curves showing the predictive efficiency of the VMRG risk scores for 1-year, 3-year and 5-year survival. (G) Train Set; (H) Test Set; (I) External Validation Set.

and ranked to determine whether expression levels changed systematically with risk score (Fig. 3A-C). Expression levels of the three genes increased significantly with increasing risk scores. The median risk score of 1.79 was used as the cut-off value, above which was the high-risk group and below which was the low-risk group, with a higher proportion of death in high-risk patients and a lower proportion of long-term survival lower in the low-risk patients. In addition, the two groups had a significant difference in prognosis. The training set, internal test set and external validation set all exhibited poorer prognostic characteristics in the high-risk group (Fig. 3D-F, $p < 0.05$). The validation results of the ROC curve are shown below: with AUCs of 0.714, 0.675 and 0.624 at 1, 3 and 5 years for the training set; AUCs of 0.737, 0.65 and 0.65 for 1, 3 and 5 years for the test set 0.737, 0.652 and 0.590 for the test set; and AUCs of 0.634, 0.625 and 0.642 for 1, 3 and 5 years for the

external validation set, and the above results indicate that the LUAD prognostic model constructed based on VM has a relatively favorable prediction effect (Fig. 3G-I).

3.4. VMRG signatures predict differences in tumor variable load and immune microenvironment

TMB is the total number of detected somatic gene coding errors, base substitutions, gene insertion or deletion errors per million bases. TMB has been detected to be intimately affiliated with the prognosis and immune microenvironment of tumor patients. To identify the relationship between TMB and the immune microenvironment in LUAD, we first compared the gene mutations in high- and low-risk cohorts, and the cross-sectional histogram showed that the mutation rate was higher in

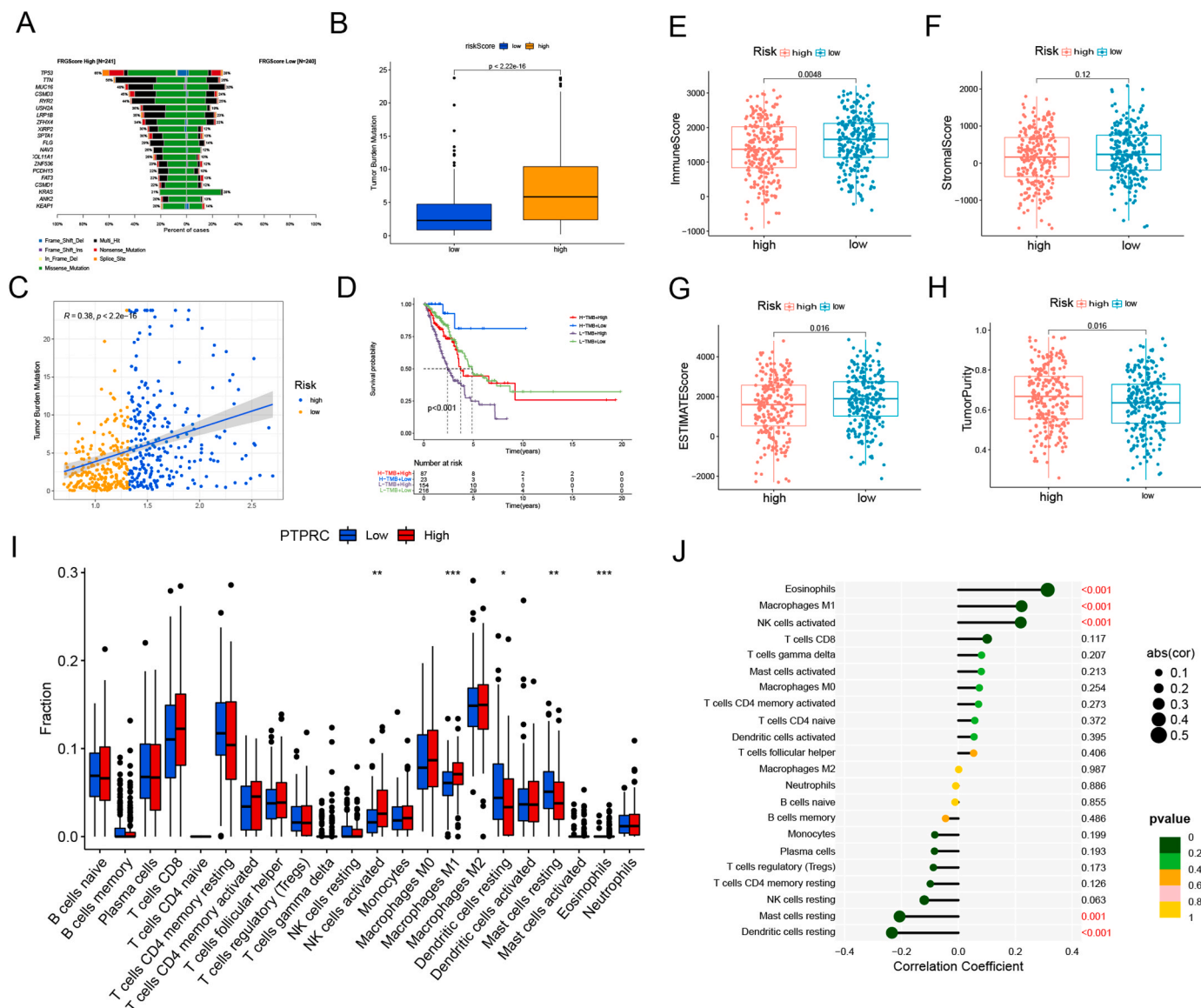


Fig. 4. The relationship between VMRG risk cohort and LUAD tumor mutation burden and immune microenvironment. (A) Mutation landscape of SMGs in TCGA-LUAD stratified by low and high VMRG score subgroups. Each column contains a proxy for individual patients. (B) Relative distribution of tumor mutational burden in high versus low subgroups of VMRG scores. (C) The correlation between TMB and VMRG risk scores, and their distribution in low- and high-risk groups. (D) Kaplan-Meier curves of TMB in combination with VMRG high and low risk groups (E-H) The immune score and tumor purity of three gene clusters were analyzed and plotted. (I) The proportion of tumor-infiltrating immune cells in the VMRG high- and low-risk cohort using the CIBERSORT algorithm. In each group, scattered dots represent the expression values of tumor microenvironment cells. The thick line represents the median value. The bottom and top of the box are the 25th and 75th percentiles (interquartile range). Statistical differences were compared by the Wilcoxon rank-sum test as follows. * $p < 0.05$; ** $p < 0.01$; *** $p < 0.001$. (J) The baton-plot shows the correlation between high and low VMRG risk scores and immune cells, with the right side representing positive correlations and the left side representing negative correlations.

the high-risk cohort than in the low-risk cohort (Fig. 4A), and further demonstrated the difference in TMB scores in the high- and low-risk cohorts (Fig. 4B). Spearman correlation analysis of positive correlation between risk score and TMB ($R = 0.36, p < 0.05$, Fig. 4C). KM survival curves demonstrated the survival status of LUAD patients in the VMRG risk cohort combined with TMB. The results showed a higher survival prognosis in the low-risk cohort with high TMB than in the high-risk cohort with low TMB ($p < 0.05$, Fig. 4D). The tumor immune microenvironment has immune cells and stromal cells as the basis for constructing the immune score, and we show the distribution of ImmuneScore, StromalScore and ESITIMATEScore and TumorPurity in the immune microenvironment in the VMRG cohort in the form of bar graphs, with ImmuneScore, StromalScore and ESITIMATEScore in the low-risk group. StromalScore and ESITIMATEScore were higher in the

low-risk group than in the high-risk group; tumor purity was higher in the high-risk group than in the low-risk group ($p < 0.05$, Fig. 4E-H). Next, we analyzed the correlation between the abundance of immune cell infiltration and the risk cohort. The results showed that plasma cells, CD4 + memory dormant cells, activated NK cells, monocytes, dormant dendritic cells, CD8 + T cells, and dormant mast cells were more enriched in the high-risk cohort. Treg cells were more infiltrated in the low-risk cohort (Fig. 4I). Eosinophils, M1 macrophages, and activated NK cells were positively correlated with risk scores, and mast cells and dormant dendritic cells were negatively correlated with risk scores (Fig. 4J).

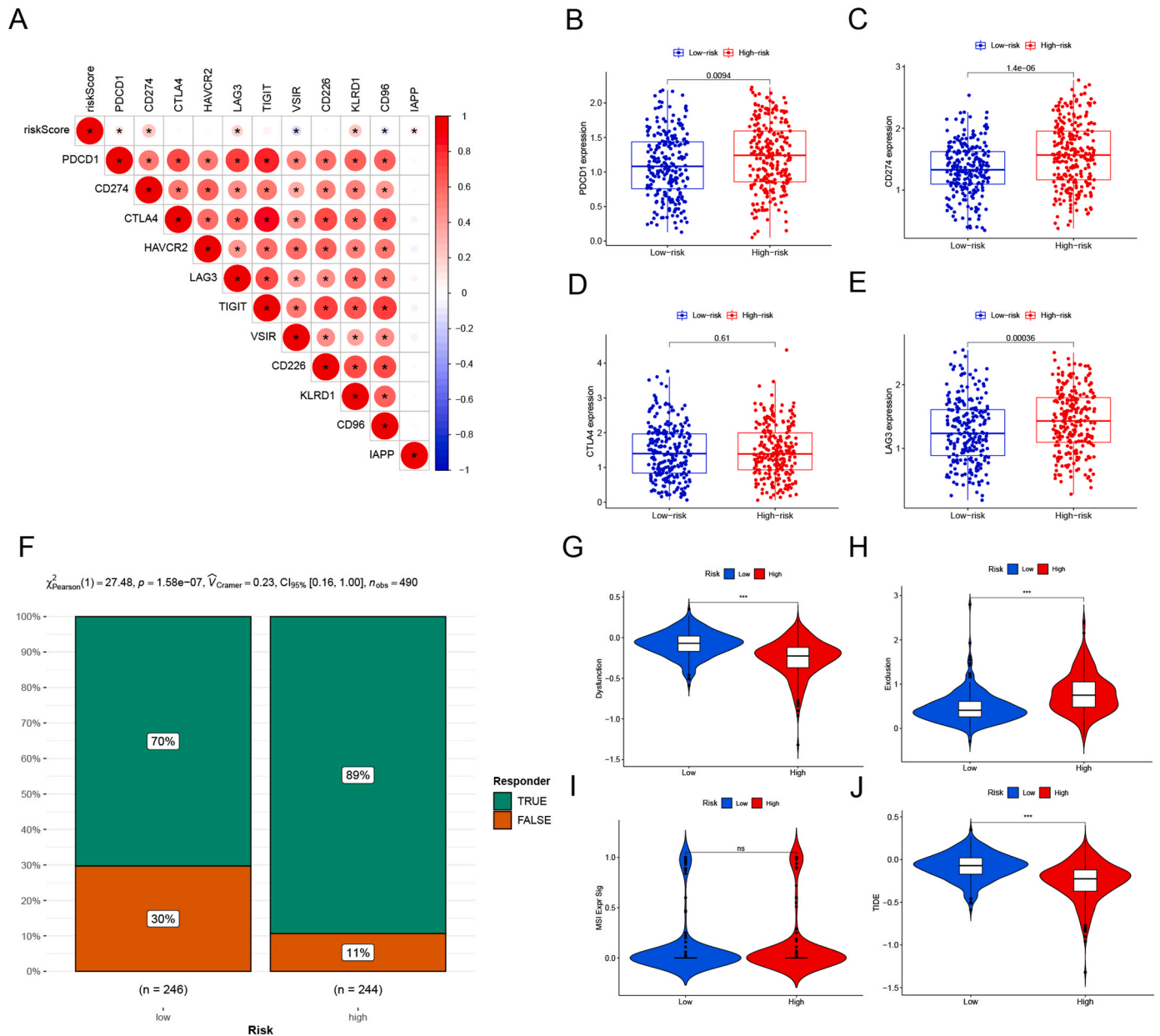


Fig. 5. The VMRG risk score predicts immunotherapeutic benefits. (A) Association of VMRG risk scores with eleven immune checkpoints, with red circles representing positive associations and blue circles representing negative associations. (B-E) Distribution of four prevalent clinical immune checkpoint molecules in VMRG high and low risk. (B) PD1; (C) PD-L1; (D) CTLA4; (E) LAG3. (F) The proportion of patients with clinical response to anti-PD1 immunotherapy in the low or high VMRG scoring group. CR/PR vs. SD/PD: 70% vs. 89% in the low VMRG score group and 30% vs. 11% in the high VMRG score group. (G-J) (G) Immunodysfunction distribution in VMRG high and low groups; (E) Immune escape distribution in VMRG high and low groups; (F) MSI distribution in VMRG high and low groups; (G) In the TCGA-LUAD, the relative distribution of TIDE was examined between the high and low VMRG groups.

3.5. Relationship between risk score and immunotherapy

As the expression of immune checkpoints affects the outcome of LUAD patients, we selected 11 immune checkpoint molecules and correlated them with risk scores to clarify the correlation (Fig. 5A). Further, we analyzed the differences in the expression of four clinically common immune checkpoint molecules in the high- and low-risk groups, and the expression of PD1, PD-L1, and LAG3 were higher in the high-risk cohort than in the low-risk cohort ($p < 0.05$, Fig. 5B-E). Next, we analyzed the proportion of immunotherapy efficacy in the risk cohort in the TIDE algorithm using a chi-square test, which showed that treatment was effective in 70% and therapy was ineffective in 30% of

the low-risk group; treatment was effective in 89% and treatment was inadequate in 11% of the high-risk group ($\chi^2 = 27.48, p < 0.05$, Fig. 5F). TIDE calculated the immunodeficiency, immune escape, microsatellite instability (MSI), and TIDE score capacity for LUAD. Immune deactivation was higher in the low-risk group than in the high-risk group, immune escape and immunotherapy efficacy were higher in the high-risk group than in the low-risk group, and there was no statistical significance in MSI scores between the two cohorts, with immunotherapy efficacy being better in the high-risk group than in the low-risk group ($p < 0.05$, Fig. 5G-J).

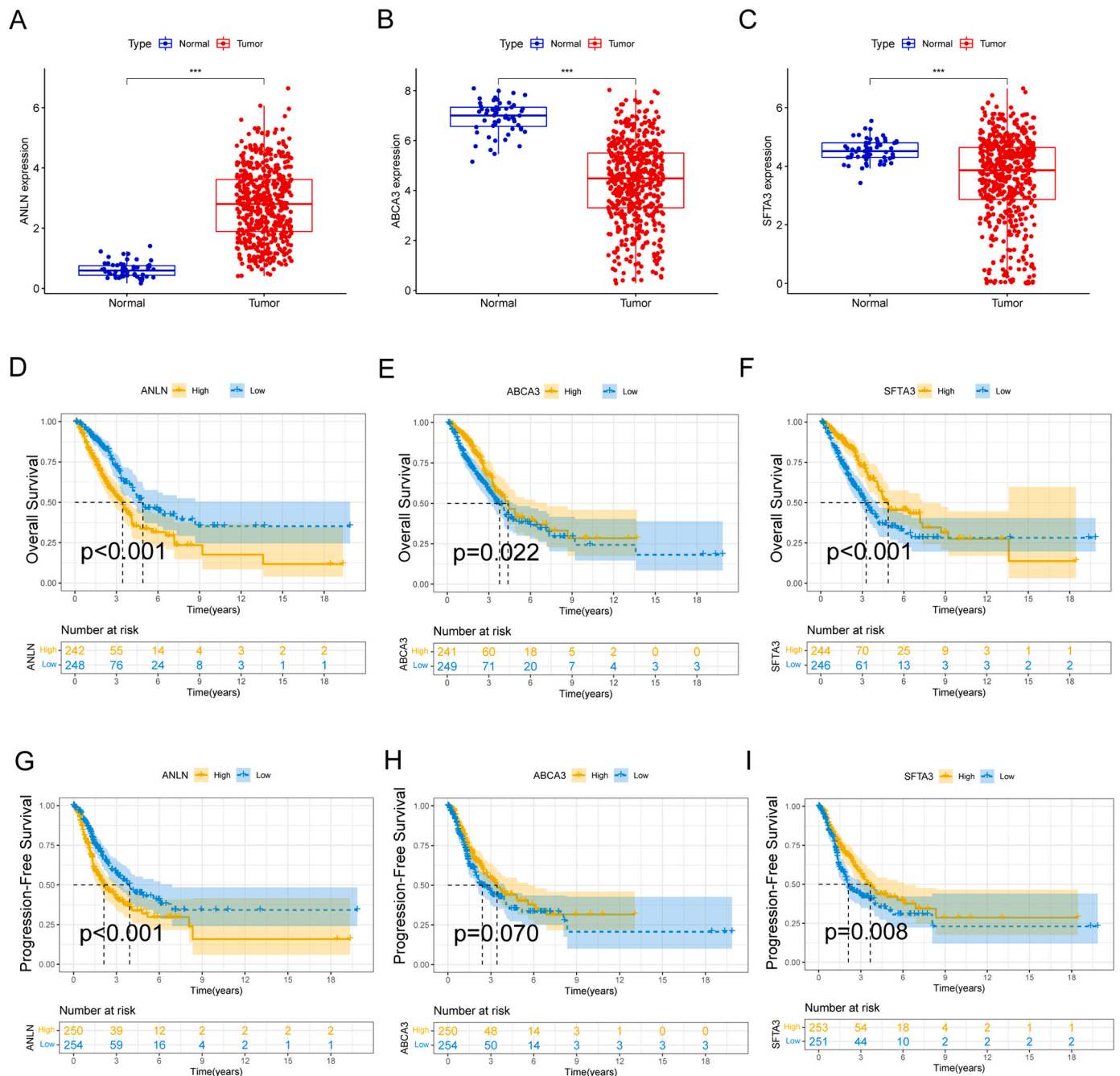


Fig. 6. Expression and prognosis of ANLN, ABCA3, SFTA3 in LUAD in the VMRG risk model. (A-C) The expression of ANLN, ABCA3, SFTA3 in cancer and pericancerous tissues. (D-F) Kaplan-Meier curves for overall survival (OS) of 490 LUAD patients in the TCGA cohort with ANLN, ABCA3, SFTA3 high and low expression cohorts. (G-I) Kaplan-Meier curves for progress-free survival (PFS) of 490 LUAD patients in the TCGA cohort with ANLN, ABCA3, SFTA3 high and low expression cohorts.

3.6. ANLN as a regulatory target of LUAD is negatively correlated with prognosis

We further evaluated the expression and survival differences of the three genes ANLN, ABCA3, and SFTA3 in LUAD in the construct VMRG model. the expression of ANLN was higher in cancer tissues than in paracancerous tissues, and ABCA3 and SFTA3 were lower in paracancerous tissues (Fig. 6A-C). The prognosis of OS was worse in the high ANLN expression group, and ABCA3 and SFTA3 low expression group

had worse OS ($p < 0.05$, Fig. 6D-F). Meanwhile, the prognosis of PFS was poorer in the ANLN high expression group and worse in the SFTA3 low expression group ($p < 0.05$, Fig. 6G-I). The above results suggest that ANLN can be a new target of LUAD to promote cancer progression.

3.7. ANLN was critical for VM formation in A549 and PC9 cells in vitro

Previous studies suggest that ANLN was hyperexpressed in tumor tissues and negatively correlated with prognosis. To elucidate the

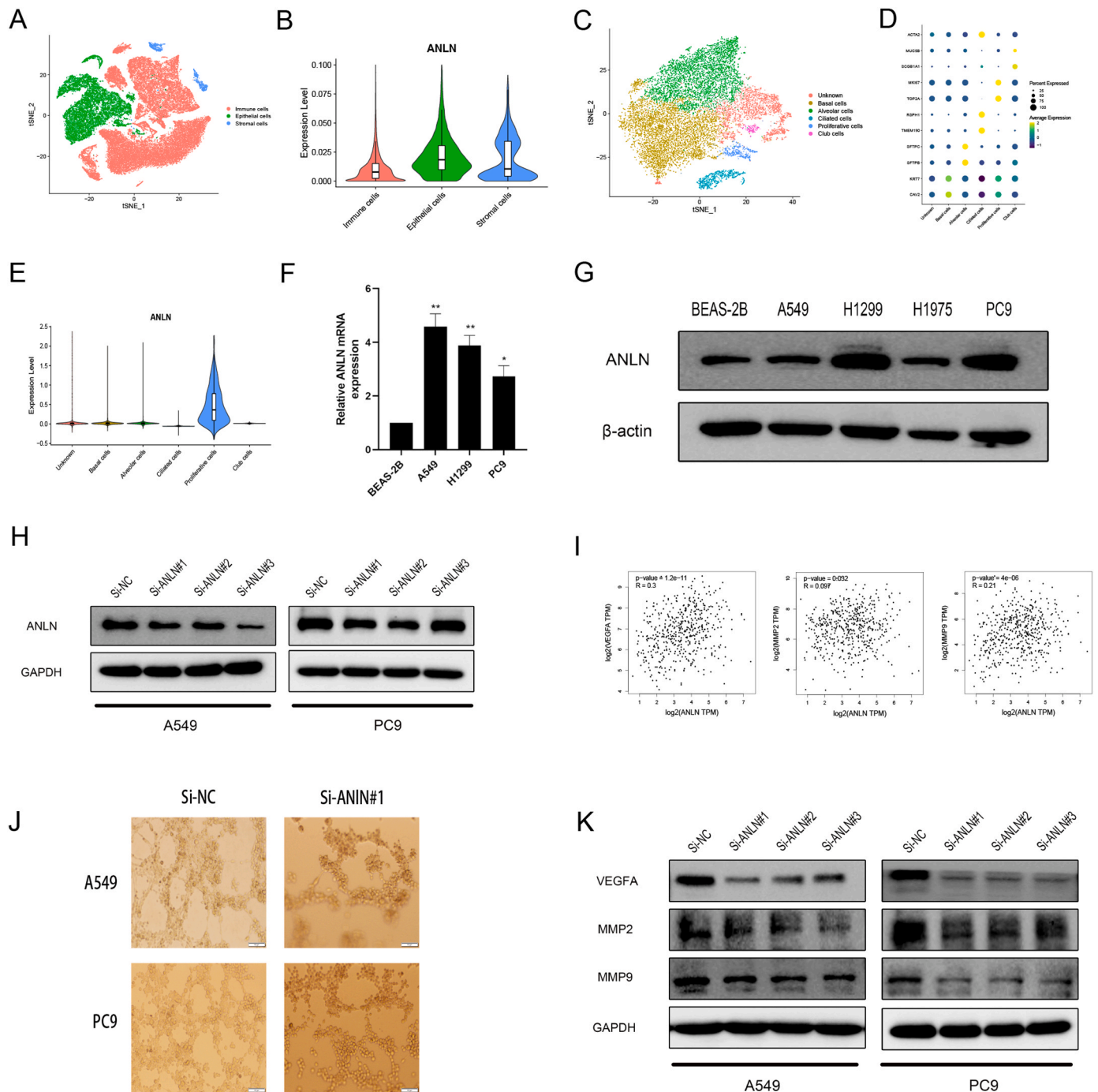


Fig. 7. ANLN knockdown significantly inhibits VM formation in A549 and PC9 cells in vitro. (A) Subcellular distribution of the LUAD single-cell dataset. (B) Expression levels of ANLN in epithelial cells, immune cells and stromal cells. (C-D) epithelial cell subtypes and mark genes for the corresponding subtypes. (E) ANLN expression in epithelial subtype cells. (F-G) The expression of ANLN was considerably elevated in NSCLC cells compared to BEAS-2B cells. (H) A549 and PC9 cells were engineered to produce ANLN-knockdown cell lines. (I) The online GEPIA exhibited a correlation between ANLN and MMP2, MMP9 and VEGFA gene expression levels. (J) The ability of VM formation in A549 and PC9 cells was significantly impaired after ANLN knockdown. (K) ANLN knockdown groups were examined for protein levels of MMP2, MMP9, and VEGFA.

distribution of ANLN in LUAD, we first selected a single-cell dataset of LUAD divided into three subpopulations of immune cells [20], Epithelial cells and Stromal cells (Fig. 7A). As previously, ANLN expression was higher on epithelial cells than on immune cells and stromal cells (Fig. 7B). Subsequently, we separated the epithelial cells into six different types of epithelial cells: Club cells, Proliferative cells, Ciliated cells, Alveolar cells, Bssal cells and Unknown. (Fig. 7C-D). The violin plots suggest that ANLN was highly expressed in Proliferative cells (Fig. 7E).

To confirm whether ANLN expression was increased in lung adenocarcinoma, we examined the expression of ANLN in lung adenocarcinoma. qPCR and protein immunoblotting results revealed that ANLN mRNA and protein expression levels were significantly higher in lung adenocarcinoma than in normal bronchial epithelial cells (Fig. 7F-G). To investigate the function of ANLN in lung adenocarcinoma and its mechanism, we used specific siRNAs in A549 and PC9 cells, thus establishing ANLN knockdown lung adenocarcinoma cell lines (Fig. 7H). VEGFA, MMP2 and MMP9 are all representative molecules of vasculogenic mimicry. We first analyzed the correlation between ANLN and VEGFA, MMP2 and MMP9 in the GEPIA database (<http://gepia.cancer-pku.cn/>), and the results showed that ANLN was positively correlated with all three ($R > 0$, $p < 0.05$, Fig. 7I). Tube-forming assays were performed with seeded cells on the substrate. The results showed that both A549NC and PC9NC cells formed vascular-like structures in the stromal culture system. However, in A549KD and PC9KD cells, we observed a significant reduction in tube formation (Fig. 7J). Further WB results showed that VEGFA, MMP2 and MMP9 decreased to different degrees when ANLN was knocked down (Fig. 7K). The above results indicate that ANLN is significantly associated with VM formation in A549 and PC9 cells.

4. Discussion

An emerging blood system for tumors, VMs are tubular networks formed by cancer cells with pluripotent and stem cell-like phenotypes that provide an adequate blood supply for solid tumor growth [21,22]. An abundant vascular supply was detected in non-small cell lung cancer tissues [23]. However, the clinical outcome of anti-angiogenic therapy was not satisfactory [24,25]. This may be due to our limited understanding of the vascular types and associated molecular mechanisms in non-small cell lung cancer. There is growing evidence that physiological perfusion between VM channels and endothelium-dependent vessels promotes tumor cell proliferation and metastasis [26,27]. VM provides an adequate blood supply to various malignancies, and VM and VM density are associated with poor prognosis and 5-year survival of tumor patients [28]. In general, VM formation in malignant tumors makes it more likely that tumor cells will migrate and infiltrate into distant tissues and organs; therefore, VM is important for predicting the course of tumors. In the process of VM formation, HIF-1 α signaling pathway [29], VEGF signaling pathway [30], Wnt/ β -catenin signaling pathway [31], MAPK signaling pathway [32], PI3K/Akt signaling pathway [33], and MMPs are involved [34,35]. Nevertheless, the specific roles of these molecular mechanisms in VM formation are still not well understood and need to be further investigated.

In the present study, we identified two different VM modification patterns with distinct immunophenotypes associated with additional anti-cancer immunity. VM-C1 was generally more abundant than VM-C2 type by infiltration. Considering the poor prognosis of the C1 type, our pathway analysis of C1 and C2 showed that the C1 type was mainly enriched in cell proliferation and metabolism related signaling pathways. A large body of literature has previously demonstrated that tumor cells use metabolic reprogramming for immune escape, which may further explain the lack of a better prognosis for C1 type despite infiltrating immune activated cells. Furthermore, differentially expressed genes (DEGs) identified from different VM modification patterns were significantly overrepresented in the biological pathways of RNA

polyadenylation and immunity, suggesting that these DEGs are thought to be the gene signature associated with the VM phenotype. Similar to the results of VM modification clustering, two transcriptome subtypes based on VM signature genes and significantly associated with different survival outcomes and TME landscapes. We further developed a quantitative system called VMRG to define different VM modification patterns and more accurately guide treatment strategies for individual patients. The results showed that our VMRG model was consistently evaluated in both the internal training set and the external validation set. Further analysis highlighted that the VMRG score is a prognostic independent risk factor for LUAD and correlates with mutation signature status, suggesting that the VMRG score may serve as a better proxy for genomic aberrations. In addition, we observed that m6Sig scores were closely associated with predictors of the immune response, including TIME, immune checkpoints, IPS and TIDE, implying that VM modifications may influence the therapeutic efficacy of immunotherapy.

Moreover, we analyzed each of the three regulators (ANLN, ABCA3 and SFTA3) in the VMRG model, and only ANLN was highly expressed in LUAD and had a poor prognosis when highly expressed. ANLN was also previously reported as an oncogene in pancreatic cancer [36], triple-negative breast cancer [37], and bladder cancer [38], promoting tumor progression. ANLN is located at 7p14.2 and encodes an actin-binding protein that plays a role in cell growth, migration, and cytoplasmic division [39,40]. Wang et al. reported that ANLN-induced upregulation of EZH2 promotes pancreatic cancer through mediating the miR-218-5p/ANLN in triple-negative breast cancer enhances triple-negative breast cancer stem cells and promotes their spheroid growth through TWIST1 and BMP2 [36]; recent studies have shown that ANLN acts as a promoter of bladder uroepithelial carcinoma by activating the JNK signaling pathway [41]. In several publications, ANLN has been reported to have a role in promoting lung cancer progression [42]. Suzuki et al. found that ANLN plays a crucial role in human lung carcinogenesis by activating RHOA and involvement in the PI3K/AKT pathway [42]. The role of ANLN in promoting tumor angiogenesis has been reported in the literature, but there is no report that ANLN regulates tumor cell generation VM. In this study, three genes downstream of ANLN were examined and VEGFA, MMP2 and MMP9 were found to be downregulated after knockdown of ANLN. Therefore, ANLN could be a new target for regulating LUAD angiogenesis mimicry.

In conclusion, it is advantageous to thoroughly investigate the role of VM in tumor growth and metastasis for clinical judgment and assessment of the staging and prognosis of associated tumors, providing more techniques for subsequent treatment and advantageous ideas for developing associated targeted drugs. Anti-tumor therapies have high possibilities for anti-angiogenic treatment paired with VM inhibition in the future.

5. Ethics approval and consent to participate

This research was approved by the Ethics Committee Board of the Second Affiliated Hospital of Bengbu Medical College.

Funding

This research was supported by The Natural Science Project of Anhui Province Senior University (KJ2021A0755); Key Project of Humanities and Social Sciences Research, Department of Education of Anhui Province (2022AH051398).

Author statement

We the undersigned declare that this manuscript entitled "Vasculogenic mimicry-associated novel gene signature predicted prognosis and response to immunotherapy in lung adenocarcinoma" is original, has not been published before and is not currently being considered for publication elsewhere. We would like to draw the attention of the Editor to

the following publications of one or more of us that refer to aspects of the manuscript presently being submitted. Where relevant copies of such publications are attached. We confirm that the manuscript has been read and approved by all named authors and that there are no other persons who satisfied the criteria for authorship but are not listed. We further confirm that the order of authors listed in the manuscript has been approved by all of us. We understand that the Corresponding Author is the sole contact for the Editorial process. He is responsible for communicating with the other authors about progress, submissions of revisions and final approval of proofs.

CRedit authorship contribution statement

LZ and JTW contributed equally to this work. The study was designed by WWY and SWW. Data analysis was carried out by LZ, JJH, and LLL. Bioinformatics analysis was conducted by LZ and ZWX. JTW and JJM provided useful advice to the analyses of the data. The manuscript was drafted by LZ and SWW, and was revised by all authors before the final version was approved to be published.

Declaration of Competing Interest

The authors declare no competing interests. LZ and JTW contributed equally to this work. The study was designed by WWY and SWW. Bioinformatics analysis was conducted by LZ and ZWX. JTW and JJM provided useful advice to the analyses of the data. The manuscript was drafted by LZ and SWW, and was revised by all authors before the final version was approved to be published.

Acknowledgements

The authors would like to credit the patients who donated samples for this study and the research team who were instrumental in generating the LUAD sample data from TCGA and GEO.

Consent for publication

Not applicable.

Appendix A. Supporting information

Supplementary data associated with this article can be found in the online version at [doi:10.1016/j.prp.2023.155048](https://doi.org/10.1016/j.prp.2023.155048).

References

- Bray, F., Ferlay, J., Soerjomataram, R.L., Siegel, L.A., Torre, A., Jemal, Global cancer statistics 2018: GLOBOCAN estimates of incidence and mortality worldwide for 36 cancers in 185 countries, *CA-A CANCER J. CLINICIANS* vol. 68 (6) (2018) 394–424.
- C.E. DeSantis, C.C. Lin, A.B. Mariotto, R.L. Siegel, K.D. Stein, J.L. Kramer, R. Alteri, A.S. Robbins, A. Jemal, Cancer treatment and survivorship statistics, 2014, *CA-A CANCER J. CLINICIANS* vol. 64 (4) (2014) 252–271.
- C. Viallard, B. Larrivée, Tumor angiogenesis and vascular normalization: alternative therapeutic targets, *ANGIOGENESIS* vol. 20 (4) (2017) 409–426.
- D.C. Singleton, A. Macann, W.R. Wilson, Therapeutic targeting of the hypoxic tumour microenvironment, *Nat. Rev. Clin. Oncol.* vol. 18 (12) (2021) 751–772.
- R.Y. Chen, C.J. Yen, Y.W. Liu, C.G. Guo, C.Y. Weng, C.H. Lai, J.M. Wang, Y.J. Lin, L.Y. Hung, "CPAP promotes angiogenesis and metastasis by enhancing STAT3 activity," *Cell Death Differ.* vol. 27 (4) (2020) 1259–1273.
- K.S. Tewari, M.W. Sill, H.J. Long 3rd, et al., Improved survival with bevacizumab in advanced cervical cancer, *N. Engl. J. Med.* vol. 370 (8) (2014) 734–743.
- D. Song, J. Lan, Y. Chen, et al., "NSD2 promotes tumor angiogenesis through methylating and activating STAT3 protein," *ONCOGENE* vol. 40 (16) (2021) 2952–2967.
- A.J. Maniotis, R. Folberg, A. Hess, E.A. Seftor, L.M. Gardner, J. Pe'er, J.M. Trent, P. S. Meltzer, M.J. Hendrix, Vascular channel formation by human melanoma cells in vivo and in vitro: vasculogenic mimicry, *Am. J. Pathol.* vol. 155 (3) (1999) 739–752.
- X. Mei, Y.S. Chen, F.R. Chen, S.Y. Xi, Z.P. Chen, "Glioblastoma stem cell differentiation into endothelial cells evidenced through live-cell imaging," *NEURO-Oncol.* vol. 19 (8) (2017) 1109–1118.
- P.M. Lical, G. Graziani, Therapeutic implication of vascular endothelial growth factor receptor-1 (VEGFR-1) targeting in cancer cells and tumor microenvironment by competitive and non-competitive inhibitors (no.), *Pharmacol. Res.* vol. 136 (2018) 97–107.
- D. Liu, J.R. Lin, E.J. Robitschek, et al., Evolution of delayed resistance to immunotherapy in a melanoma responder, *Nat. Med.* vol. 27 (6) (2021) 985–992.
- Y. Wang, X. Song, Y. Zheng, Z. Liu, Y. Li, X. Qian, X. Pang, Y. Zhang, Y. Yin, "Cancer/testis Antigen MAGEA3 Interacts with STAT1 and Remodels the Tumor Microenvironment," *Int. J. Med. Sci.* vol. 15 (14) (2018) 1702–1712.
- J. Xu, X. Yang, Q. Deng, et al., TEM8 marks neovasculogenic tumor-initiating cells in triple-negative breast cancer, *Nat. Commun.* vol. 12 (1) (2021) 4413.
- Q. She, S. Hu, X. Pu, Q. Guo, C. Mou, C. Yang, "The effect of hepatocellular carcinoma-associated fibroblasts on hepatoma vasculogenic mimicry," *Am. J. Cancer Res.* vol. 10 (12) (2020) 4198–4210.
- Q. Liu, E. Zhao, B. Geng, S. Gao, H. Yu, X. He, X. Li, G. Dong, B. You, "Tumor-associated macrophage-derived exosomes transmitting miR-193a-5p promote the progression of renal cell carcinoma via TIMP2-dependent vasculogenic mimicry," *Cell Death Dis.* vol. 13 (4) (2022) 382.
- A. Newman, C.L. Liu, M.R. Green, A.J. Gentles, W. Feng, Y. Xu, C.D. Hoang, M. Diehn, A.A. Alizadeh, Robust enumeration of cell subsets from tissue expression profiles, *Nat. METHODS* vol. 12 (5) (2015) 453–457.
- A. Subramanian, P. Tamayo, V.K. Mootha, et al., "Gene set enrichment analysis: a knowledge-based approach for interpreting genome-wide expression profiles," *Proc. Natl. Acad. Sci. USA* vol. 102 (43) (2005) 15545–15550.
- P. Jiang, S. Gu, D. Pan, et al., "Signatures of T cell dysfunction and exclusion predict cancer immunotherapy response," *Nat. Med.* vol. 24 (10) (2018) 1550–1558.
- M.I. Love, W. Huber, S. Anders, Moderated estimation of fold change and dispersion for RNA-seq data with DESeq2, *GENOME Biol.* vol. 15 (12) (2014), 550.
- P. Bischoff, A. Trinks, B. Obermayer, et al., "Single-cell RNA sequencing reveals distinct tumor microenvironmental patterns in lung adenocarcinoma," *ONCOGENE* vol. 40 (50) (2021) 6748–6758.
- Q. Luo, J. Wang, W. Zhao, et al., "Vasculogenic mimicry in carcinogenesis and clinical applications," *J. Hematol. Oncol.* vol. 13 (1) (2020) 19.
- X. Wei, Y. Chen, X. Jiang, et al., Mechanisms of vasculogenic mimicry in hypoxic tumor microenvironments, *Mol. Cancer* vol. 20 (1) (2021) 7.
- Z. Ma, K. Wei, F. Yang, et al., "Tumor-derived exosomal miR-3157-3p promotes angiogenesis, vascular permeability and metastasis by targeting TIMP/KLF2 in non-small cell lung cancer," *Cell Death Dis.* vol. 12 (9) (2021) 840.
- E.A. Kuczynski, P.B. Vermeulen, F. Pezzella, R.S. Kerbel, A.R. Reynolds, Vessel co-option in cancer, *Nat. Rev. Clin. Oncol.* vol. 16 (8) (2019) 469–493.
- Q. Li, Y. Wang, W. Jia, et al., "Low-Dose Anti-Angiogenic Therapy Sensitizes Breast Cancer to PD-1 Blockade," *Clin. CANCER Res.* vol. 26 (7) (2020) 1712–1724.
- H.Y. Wan, Q.Q. Li, Y. Zhang, W. Tian, Y.N. Li, M. Liu, X. Li, H. Tang, miR-124 represses vasculogenic mimicry and cell motility by targeting amotL1 in cervical cancer cells, *CANCER Lett.* vol. 355 (no. 1) (2014) 148–158.
- Y. Wang, L. Tong, J. Wang, et al., cRGD-functionalized nanoparticles for combination therapy of anti-endothelium dependent vessels and anti-vasculogenic mimicry to inhibit the proliferation of ovarian cancer (no.), *Acta Biomater.* vol. 94 (2019) 495–504.
- Z. Cao, M. Bao, L. Miele, F.H. Sarkar, Z. Wang, Q. Zhou, "Tumour vasculogenic mimicry is associated with poor prognosis of human cancer patients: a systemic review and meta-analysis," *Eur. J. CANCER* vol. 49 (18) (2013) 3914–3923.
- M. Wang, X. Zhao, D. Zhu, T. Liu, X. Liang, F. Liu, Y. Zhang, B. Sun, "HIF-1 α promoted vasculogenic mimicry formation in hepatocellular carcinoma through LOXL2 up-regulation in hypoxic tumor microenvironment," *J. Exp. Clin. CANCER Res.* vol. 36 (1) (2017) 60.
- Y. Chen, L. Zhang, W.X. Liu, K. Wang, VEGF and SEMA4D have synergistic effects on the promotion of angiogenesis in epithelial ovarian cancer (no.), *Cell. Mol. Biol. Lett.* vol. 23 (2018) 2.
- L. Qi, W. Song, Z. Liu, X. Zhao, W. Cao, B. Sun, "Wnt3a Promotes the Vasculogenic Mimicry Formation of Colon Cancer via Wnt/ β -Catenin Signaling," *Int. J. Mol. Sci.* vol. 16 (8) (2015) 18564–18579.
- M.A. Nisar, Q. Zheng, M.Z. Saleem, B. Ahmmed, M.N. Ramzan, S.R. Ud Din, N. Tahir, S. Liu, Q. Yan, IL-1 β Promotes Vasculogenic Mimicry of Breast Cancer Cells Through p38/MAPK and PI3K/Akt Signaling Pathways (no.), *Front. Oncol.* vol. 11 (2021), 618839.
- Y. Zhu, X. Liu, P. Zhao, H. Zhao, W. Gao, L. Wang, Celestrol Suppresses Glioma Vasculogenic Mimicry Formation and Angiogenesis by Blocking the PI3K/Akt/mTOR Signaling Pathway (no.), *Front. Pharmacol.* vol. 11 (2020) 25.
- W. Zhu, W. Sun, J.T. Zhang, Z.Y. Liu, X.P. Li, Y.Z. Fan, Norcantharidin enhances TIMP-2 anti-vasculogenic mimicry activity for human gallbladder cancers through downregulating MMP-2 and MT1-MMP, *Int. J. Oncol.* vol. 46 (2) (2015) 627–640.
- F. Yang, M. Wen, D. Pan, X. Lin, J. Mo, X. Dong, S. Liao, Y. Ma, IL-33/ST2 Axis Regulates Vasculogenic Mimicry via ERK1/2-MMP-2/9 Pathway in Melanoma, *DERMATOLOGY* vol. 235 (3) (2019) 225–233.
- A. Wang, H. Dai, Y. Gong, C. Zhang, J. Shu, Y. Luo, Y. Jiang, W. Liu, P. Bie, "ANLN-induced EZH2 upregulation promotes pancreatic cancer progression by mediating miR-218-5p/LASP1 signaling axis," *J. Exp. Clin. CANCER Res.* vol. 38 (1) (2019) 347.
- X. Dai, Y. Mei, X. Chen, D. Cai, ANLN and KDR Are Jointly Prognostic of Breast Cancer Survival and Can Be Modulated for Triple Negative Breast Cancer Control (no.), *Front. Genet.* vol. 10 (2019), 790.
- S. Wu, K. Nitschke, J. Heinkelde, C.A. Weis, T.S. Worst, M. Eckstein, S. Porubsky, P. Erben, ANLN and TLE2 in Muscle Invasive Bladder Cancer: A Functional and

- Clinical Evaluation Based on In Silico and In Vitro Data, *Cancers (Basel)* vol. 11 (12) (2019).
- [39] N.M. Tuan, C.H. Lee, Role of Anillin in Tumour: From a Prognostic Biomarker to a Novel Target, *Cancers (Basel)* vol. 12 (6) (2020).
- [40] N.G. Naydenov, J.E. Koblinski, A.I. Ivanov, Anillin is an emerging regulator of tumorigenesis, acting as a cortical cytoskeletal scaffold and a nuclear modulator of cancer cell differentiation, *Cell Mol. Life Sci.* vol. 78 (2) (2021) 621–633.
- [41] S. Zeng, X. Yu, C. Ma, et al., Transcriptome sequencing identifies ANLN as a promising prognostic biomarker in bladder urothelial carcinoma, *Sci. -ic Rep.* vol. 7 (1) (2017), 3151.
- [42] C. Suzuki, Y. Daigo, N. Ishikawa, T. Kato, S. Hayama, T. Ito, E. Tsuchiya, Y. Nakamura, "ANLN plays a critical role in human lung carcinogenesis through the activation of RHOA and by involvement in the phosphoinositide 3-kinase/AKT pathway", *CANCER Res.* vol. 65 (24) (2005) 11314–11325.